Modeling, Identification and Control, Vol. 44, No. 3, 2023, pp. 111–124, ISSN 1890–1328

# Improving Energy Efficiency and Response Time of an Offshore Winch Drive with Digital Displacement Motors

Thomas Farsakoglou* [1] Henrik C. Pedersen [1] Morten K. Ebbesen [2] Torben O. Andersen [1]

[1] *Department of Energy, Aalborg University, 9220 Aalborg, Denmark. E-mail:* {thfa*, hcp, toa}@energy.aau.dk

[2] *Faculty of Engineering and Science, University of Agder, Postbox 422, 4604 Kristiansand, Norway. E-mail:* morten.k.ebbesen@uia.no

**Abstract**

Offshore winch drives require high energy efficiency and control precision, making digital displacement motors an attractive solution due to their high efficiency and potential controllability. However, the response time and the realized energy efficiency of these motors are heavily dependent on the chosen displacement control strategy, especially at low-speed operation. This paper considers various displacement control strategies to investigate whether digital displacement motors are a viable solution for offshore winch drive applications. The motor specifications are derived based on the requirements of a commercial offshore winch drive system. The analysis reveals that various displacement control strategies should be used across the drive's operational speed range to ensure both satisfactory performance and high efficiency. Full-stroke and partial-stroke strategies are optimal for speeds above 28 rpm and 20 rpm, respectively, but unsuited for lower-speed operation. For speeds below 20 rpm, an improved sequential-stroke strategy is therefore presented. The proposed displacement control strategy provides instantaneous motor response and maintains high energy efficiency, although its robustness is slightly reduced at higher operating speeds above 20 rpm.

*Keywords:* Offshore, Digital Hydraulics, Winch Drive, Energy Efficiency, Valves

## 1 Introduction

Offshore cranes widely rely on winch drives to handle loads accurately in the harsh maritime environment. Such loads typically weigh hundreds of tons and are handled at very low translational speeds, generally below 8 m/min. An example of a commercial offshore knuckle-boom crane rated for lifting up to 150 t is shown in Figure 1. The winch drive controls the load's vertical position when it is suspended from the hook and can be raised or lowered by paying out or reeling in the wire. As the offshore industry seeks to meet various environmental criteria, improving the energy efficiency of these drives has become increasingly important. Digital displacement motors (DDMs)—a complete list of abbreviations can be found at the end of the paper — have emerged as promising candidates for enhancing offshore winch drive efficiency. Hydraulic DDMs can drastically reduce leakage, friction, and compressibility losses compared to conventional hydraulic motors, as the flow to each piston is individually controlled by a pair of digital valves.

A detailed description of digital displacement pumps and motors can be found in previous research (Nordås, 2020; Pedersen, 2018; Nørgård, 2017; Roemer, 2014; Merrill, 2012). The efficiency and response time of DDMs are highly dependent on the valve timing control. The valve timing control strategy affects how

doi:10.4173/2023.3.2

the piston strokes are controlled and, consequently, the displacement control strategy. Various displacement control strategies have been proposed and can be broadly classified into three categories: full-stroke, partial-stroke, and sequential partial-stroke. The efficiency and response time of the various strategies have been investigated in various papers (Payne et al., 2007; Merrill, 2012; Heikkilä et al., 2010; Rømer et al., 2013; Nørgård, 2017; Williamson and Manring, 2019). However, these studies consider digital displacement machines operating at high speeds i.e., above 500 rpm.


Figure 1: Offshore knuckle-boom NOV crane, rated for lifting up to 150 t loads.

In a review of these strategies by Pedersen et al. (2018a), it was shown that the appropriate displacement strategy depends on the chosen application. The results showed that for high-speed operation, a full-stroke strategy provides a low response time and high energy efficiency. At medium to low speeds, a partial-stroke strategy offers a faster response at lower displacements as it uses all cylinders to reach the desired displacement; however, the energy efficiency decreases. For very-low speeds, the sequential partial-stroke strategy offers a fast response which is limited only by the actuation time of the valves, but energy losses are significantly increased. A method that is referred to as creep mode was introduced by Larsen et al. (2018) for controlling DDMs at very low speeds. The method belongs to the sequential partial-stroke category and relies on slowly moving the motor's shaft from one force equilibrium to the next by pressurizing or depressurizing one chamber at a time. High position accuracy can be achieved using this method; however, the energy efficiency was not evaluated. Larsen et al. note that at fast shaft speeds, the method can impose wear on the valves and the electrical system due to the resulting high frequency of valve switching. Nordås et al. (2019), analyzed the behavior and response time of DDMs for a winch drive. The results show that both full-stroke and partial-stroke strategies have a very slow response for a low-speed application such as offshore winch drives. A sequential-stroke strategy provided a fast response but required more frequent switching of the digital valves. To overcome these issues, Nordås et al. proposed a particular case of a sequential partial-stroke strategy. The method closely resembles a conventional partial-stroke strategy. However, when the displacement reference is increased, any piston that is able to contribute torque toward the desired direction is allowed to switch the states of the valves to pressurize the chamber regardless of the shaft position. The method allows the motor to respond quickly without requiring frequent valve actuation. However, the authors did not evaluate the energy efficiency of this method.

Presently, no existing studies have addressed the response time requirements of DDMs within the context of a winch drive application, based on either a commercially available system or a prototype winch drive system. Furthermore, there is a lack of control strategies for DDMs that simultaneously provide low response times at low speeds while sustaining a high volumetric efficiency. These represent substantial gaps in the current understanding and application of DDMs for low speed applications.

This paper provides an overview of how the different displacement stroke strategies can be utilized to allow an offshore winch drive to maintain low response time, as defined in Section 2, and high energy efficiency throughout its operating range. For that purpose, the method proposed by Nordås et al. (2019) for reducing the response time of the motors is evaluated and improved with respect to energy efficiency. The new method allows DDMs to respond fast at very low speeds while maintaining high energy efficiency. However, the method's robustness is reduced at hiegher shaft speeds. The offshore winch drive under consideration was first introduced by Farsakoglou et al. (2022) and is designed based on a commercial winch drive system by NOV, a worldwide leading manufacturer of offshore cranes and winch drive systems (NOV, 2022). In this paper, the conventional hydraulic motors and their gearboxes have been replaced with digital displacement motors. Therefore, the response time requirement is obtained from the response characteristics of the conventional motors that are used for the commercial drive.

This paper is structured as follows. Section 2 provides an overview of the commercial winch drive system and the considered winch drive that utilizes digital displacement motors. The methodology for modeling the digital displacement motors is presented in Section 3, followed by the description of the considered displacement control strategies in Section 4. The response time offered by each displacement control strategy across the drive's operating speed range is investigated in Section

5. The resulting energy efficiency for each strategy is discussed in Section 6. It is found that the simplified sequential-stroke strategy, proposed in previous work, offers low response time but significant losses. Therefore, Section 7 describes a new methodology used to limit these losses, and the modified sequential-stroke strategy is compared to the original method in Section 8, where it is shown to significantly improve energy efficiency. Finally, Section 9 summarizes the study's conclusions.

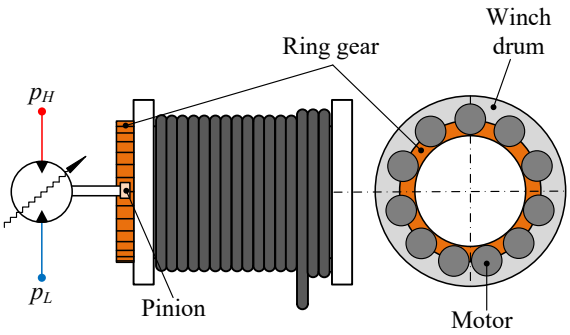


Figure 3: Simplified illustration of the considered offshore digital winch drive

## 2 Commercial & Digital Winch Drive Concept

An illustration of the original winch drive is shown in Figure 2.

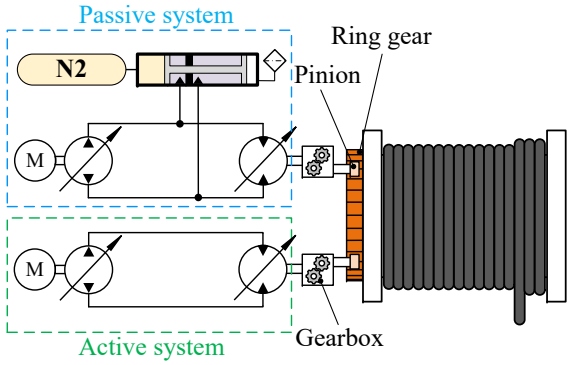


Figure 2: Simplified illustration of the commercial offshore winch drive manufactured by NOV. Inspired by Moslått et al. (2020).

The drive can be divided into two systems: an active system and a passive system, indicated by the green and blue boxes, respectively. The two systems operate in parallel and are connected to the same ring gear. The passive system operates with secondary control where the pressure in the lines is kept at a quasi-constant level. The motors adjust their displacement to produce a constant torque that negates the gravitational torque produced by the load. The active system is tasked with following the velocity reference from the crane operator while compensating for friction and external disturbances.

The proposed drive is referred to as a digital winch drive and is shown in Figure 3.

The supply for the DDMs is assumed to consist of a constant pressure for both the high- and low-pressure lines, $p_H$, and $p_L$, respectively. To connect the motors to the winch drum, only a pinion-to-ring gear connection is used. A representation of a digital displacement motor with five pistons is seen in Figure 4.

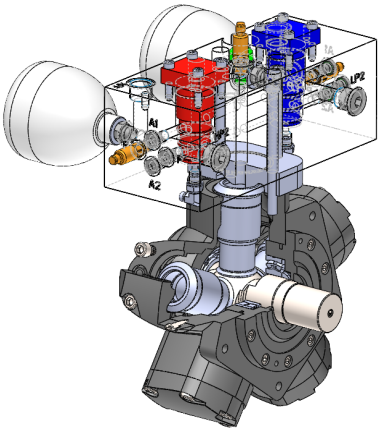

Figure 4: Model of a five-piston radial piston motor with one chamber connected to a pair of digital valves.

The considered digital displacement motors have seven cylinders that are uniformly distributed around the shaft's center of rotation, as shown in Figure 5. Each of the chambers is controlled with a pair of digital valves as shown in Figure 6. The original drive utilizes A6VM 215 motors that have been reported to have a response time from zero to maximum displacement that varies from 0.7 s to 3.5 s depending on the control pressure, control setting, and direction (Moslått et al., 2019). Therefore, the DDMs need to have a comparable response time throughout the whole operation range to maintain a similar performance.

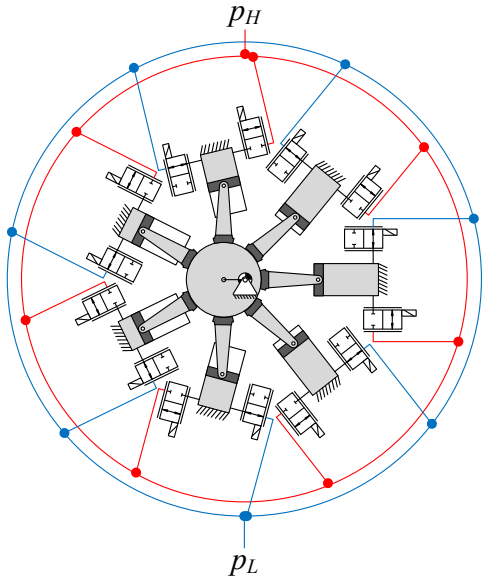


Figure 5: Simplified illustration of a digital displacement motor with seven pistons.

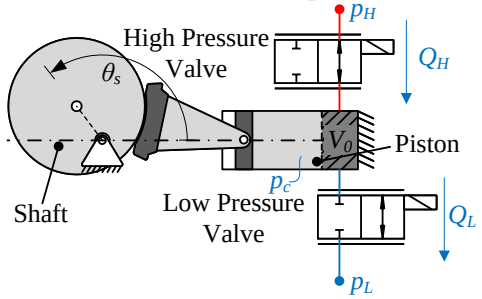


Figure 6: Sketch of a single piston of the considered digital displacement motor.

The main disturbance that offshore winch drives must compensate for is wave-induced heave motion which causes the crane's tip to oscillate vertically. The JONSWAP wave spectrum, as described by DNV (2011), is commonly used to model this type of motion. Using this spectrum, Figure 7 illustrates an example of the resulting wave-induced vertical crane tip motion that the winch system must compensate for.

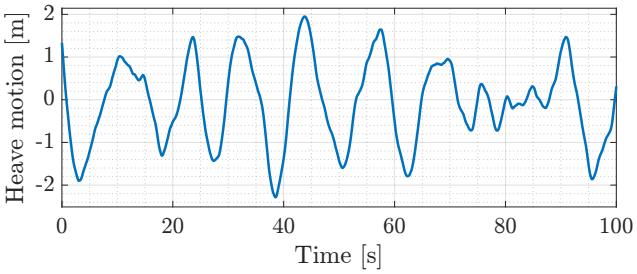


Figure 7: Example of wave-induced heave motion at the tip of the crane, generated with the JONSWAP wave spectrum.

The offshore industry requires the winch drives to be able to compensate for heave motion so that the load's position deviates no more than ±100 mm from the reference. Therefore, it is desired to utilize displacement strategies that will enable the DDMs to have a response time, i.e. reach maximum displacement from zero and vice versa, which is similar to that of the conventional motors. For that purpose, the conventional motor's average response time is selected, corresponding to approximately 1.5 s. The chosen response time requirement serves as a reference in order to evaluate and provide insights for the performance of the various displacement control strategies in Section 5. Therefore, more detailed investigations are required for specific application conditions.

As the main motivation for using DDMs is to increase the energy efficiency of the drive, it is vital to ensure that the motors maintain high energy efficiency at all points of operation. The selection of an appropriate valve is, therefore, vital for ensuring that a DDM operates with high efficiency. For this purpose, a poppet valve produced by Diinef (2023) is selected, as it is the best-suited commercially available valve. The Diinef valve offers a high flow rate for a short switching time; the valve parameters are shown in Table 1. Additionally, the valve can open against a large pressure difference across the valve, which increases the controllability of the pistons. The number of pistons for the DDMs is derived from previous work where it was shown that for the considered digital winch drive and the Diinef valve, the DDMs have a minimum efficiency of 90% energy efficiency (Farsakoglou et al., 2022). Based on these results, the lowest efficiency of 90 % occurs when the DDM operates at its maximum allowed speed with 25 % displacement produced with partial strokes. The parameters for the digital displacement motors and the digital winch drive can be found in Table 1.

## 3 DDM Modeling

By virtue of the uniform arrangement of the cylinders and the cylinders being identical, the motor's operational characteristics can be accurately modeled based on Figure 6 and then repeated for the other cylinders. As such, the pistons share a common shaft speed denoted by $\dot{\theta}_s$, while the shaft angle $\theta_{s,i}$ imparts a relative phase shift upon each piston, as represented by Eq. (1).

$$\theta_{s,i} = \theta_s - \frac{2\pi}{N_c}(i-1) \tag{1}$$

$$\dot{\theta}_{s,i} = \dot{\theta}_s \qquad i \in \{1, \ldots, N_c\} \tag{2}$$

$N_c$ and the following parameters here refer to the parameters shown in Table 1. Each chamber's pres-

Table 1: Parameters for the digital displacement motors, digital valves, and winch drive.

| **Digital Winch Drive Parameters** | | | |
|---|---|---|---|
| Symbol | Description | Value | Unit |
| $\gamma_{pr}$ | pinion to ring gear ratio | 14.17 | - |
| $N_m$ | Number of motors | 11 | - |
| | Max. operating motor velocity | 74 | rpm |
| | Min. operating motor velocity | 2 | rpm |
| **DDM Parameters** | | | |
| Symbol | Description | Value | Unit |
| $\beta_{oil}$ | Oil bulk modulus | 15000 | bar |
| $p_H$ | High pressure | 330 | bar |
| $p_L$ | Low pressure | 25 | bar |
| $V_0$ | Piston dead volume | 55 | $cm^3$ |
| $V_d$ | Piston displacement volume | 1100 | $cm^3$ |
| $N_c$ | Number of cylinders | 7 | - |
| **Digital Valve Parameters** | | | |
| $t_s$ | Switching time | 25 | ms |
| $k_f$ | Flow coefficient | 32000 | $\min\sqrt{\text{bar}}/\text{cm}^2$ |

sure dynamics are characterized by the fluid flow through the high-pressure valve $Q_{H,i}$, low-pressure valve $Q_{L,i}$, and the piston's displacement, as represented by Eq. (3).

$$\dot{p}_{c,i} = \frac{\beta_{oil}}{V_{c,i}} \left( Q_{H,i} - Q_{L,i} - \dot{V}_{c,i} \right) \tag{3}$$

$$Q_{H,i} = \frac{\bar{x}_{H,i}}{k_f} \sqrt{|p_H - p_{c,i}|} \text{sign}\left(p_H - p_{c,i}\right), \tag{4}$$

$$Q_{L,i} = \frac{\bar{x}_{L,i}}{k_f} \sqrt{|p_{c,i} - p_L|} \text{sign}\left(p_{c,i} - p_L\right) \tag{5}$$

The cylinder's volume $V_{c,i}$, volumetric flow rate $\dot{V}_{c,i}$, and shaft torque $T_{c,i}$ are functions of the piston's displacement, with the latter being additionally affected by the cylinder's internal pressure.

$$V_{c,i} = V_0 + \frac{V_d}{2}\left(1 - \cos\theta_{s,i}\right) \tag{6}$$

$$\dot{V}_{c,i} = \frac{V_d}{2}\dot{\theta}_s \sin\theta_{s,i} \tag{7}$$

$$T_{c,i} = \frac{V_d}{2} p_{c,i} \sin\theta_{s,i} \tag{8}$$

The total torque output of the winch drive $T_w$ is given as,

$$T_w = N_m \gamma_{pr} \sum_{i=1}^{N_c} T_{c,i} \tag{9}$$

The valves' movement is modeled by a sigmoid function. Therefore, when the valve closes, it has a constant negative acceleration for the first half of its switching time and a constant positive acceleration for the other half as shown in Eq. (10). The signs of the piecewise function are reversed when opening the valve. This model has been used by various studies (Rømer et al., 2013; Pedersen et al., 2020) and seems to correspond well with the results presented by Lindholdt et al. (2017):

$$\bar{x} = \int_{t_0}^{t_0+t_s} \int_{t_0}^{t_0+t_s} \epsilon \, \mathrm{d}t\mathrm{d}t \tag{10}$$

$$\epsilon = \begin{cases} -\dfrac{4}{t_s^2} & \text{for} \quad t_0 < t < \dfrac{t_s}{2} + t_0 \\ \dfrac{4}{t_s^2} & \text{for} \quad \dfrac{t_s}{2} + t_0 \leq t < t_s + t_0 \end{cases} \tag{11}$$

where $\epsilon$ is the acceleration of the valve's plunger, and $\bar{x}$ is the normalized valve plunger position.

## 4 Displacement Control Strategies

The three displacement control strategies that are considered to evaluate the motor response are briefly outlined in this section using Figure 8. More elaborate descriptions for the strategies can be found in Merrill (2012) and Pedersen (2018). Figure 8 shows the simplified pressure and flow behavior of a single cylinder based on the valve actuation sequences produced

by each displacement strategy over a revolution. The valve states are shown at the bottom of each figure, while the resulting flow and pressure are illustrated at the top.

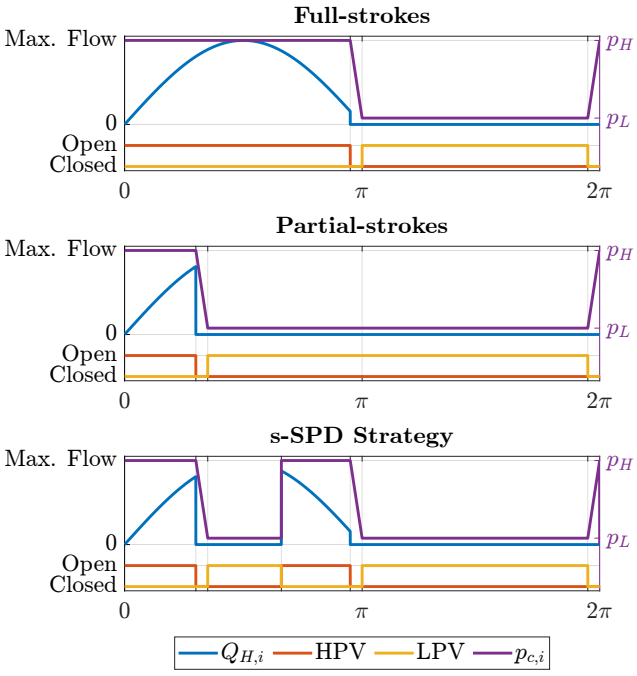


Figure 8: Illustration of the considered displacement control strategies.

A full-stroke strategy relies on activating a certain number of cylinders over one revolution to control the displacement. The number of active cylinders results in the motor's displacement over a revolution. For example, if only one cylinder is activated, the motor's displacement is equal to $1/N_c = 14\,\%$. This results in the motor's displacement becoming discrete, and therefore, intermediate displacement values can only be achieved over multiple rotations.

For an active cylinder, the high-pressure valve (HPV) is opened when the shaft is at $\theta_s = 0$, and the low-pressure valve (LPV) is opened at $\theta_s = \pi$, corresponding to the points where the flow reaches its minimum. To prevent the valves from opening against high pressure, the HPV and LPV are closed prior to the shaft reaching 0 and $\pi$, respectively. This allows the chamber to be pressurized or depressurized, thus equalizing the pressure across the HPV or LPV, respectively, before opening. Any cylinders that were not activated are referred to as idling. In an idling cylinder, the HPV remains closed, and the LPV open throughout the entire stroke. As an idling cycle does not require the chamber to be pressurized, the decision to activate or idle a cylinder is made at a fixed angle prior to the angle where the LPV closes.

A partial-stroke strategy always activates all cylinders when a non-zero displacement is requested; however, the HPV closing angle varies to control the displacement over a revolution. This results in a continuous motor displacement related to the HPV's closing angle. At zero displacement, all HPVs remain closed, and the LPVs open. Similarly to a full-stroke strategy, the decision to close the LPV in order to pressurize the chamber is made at a fixed angle prior to the LPV closing angle. In principle, a partial stroke can occur at any shaft position between 0 and $\pi$. However, the aforementioned method is widely preferred as it minimizes volumetric losses because the HPV is opened at the lowest flow, and the chamber can be pressurized prior to the HPV opening.

Sequential partial-stroke strategies switch the valves multiple times over a stroke to achieve the desired displacement. This essentially means that any number of cylinders can be activated at any time instance to provide the desired displacement. For a seven-cylinder motor that corresponds to $2^{N_c} = 128$, possible configurations of active and idle cylinders. However, previous studies have shown that such a method leads to frequent valve switchings and significant energy losses (Pedersen et al., 2018a; Nordås et al., 2019). Therefore, a simplified sequential partial-stroke displacement strategy (s-SPD) is considered as proposed by Nordås et al. (2019). The proposed strategy works similarly to a partial-stroke strategy but allows the HPV to reopen when a larger displacement is requested. For example, based on Figure 8, when using a partial stroke strategy and assuming that the displacement reference is increased to 100 % at a shaft angle of $2\pi/3$, the strategy can only open the HPV and allow flow into the chamber when the shaft reaches 0. However, the s-SPD strategy can immediately open the HPV while simultaneously closing the LPV, thus allowing flow into the chamber nearly instantaneously.

# 5 Motor Response based on Displacement Strategy

As discussed in Section 2, it is essential to ensure that the drive's torque response time from zero to maximum torque and vice versa remains lower than the average response time of the conventional winch drive, which corresponds to approximately 1.5 s. Previous studies have shown that when utilizing full-stroke or partial-stroke strategies, the DDM's displacement response is inversely proportional to its rotating speed (Nordås et al., 2019; Pedersen et al., 2018a). Therefore the slowest torque response for the winch, when using these strategies, occurs at its lowest operating speed, which is the basis for this analysis. For the con-

sidered drive, the slowest operation speed corresponds to 2 rpm. For all the figures shown in the following subsections, the reference signal change is given at $t = 0$, and the motor shaft angle is shown at the top x-axis.

## 5.1 Full-Stroke Response

For the full-stroke strategy, the decision for which cylinders should be activated is made with a first order delta-sigma modulator that was introduced by Johansen et al. (2015) and used in other publications (Pedersen et al., 2016, 2017, 2018b, 2020). The modulator translates a continuous signal to a digital with a value of 1 corresponding to an active cylinder and 0 to an idle cylinder. The implementation of a first order delta-sigma modulator is shown in Figure 9.

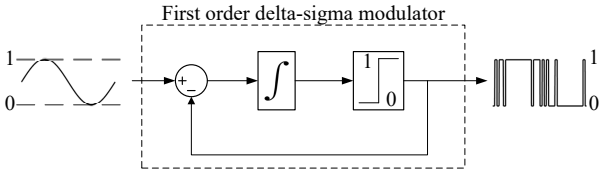


Figure 9: Configuration of a first order delta-sigma modulator, inspired by Nordås et al. (2019).

As the decision for activating a cylinder is made at a fixed angle, the sampling rate of the delta-sigma modulator $f_{\Delta\Sigma}$ is proportional to the number of pistons $N_c$ and the shaft speed $\dot{\theta}_s$,

$$f_{\Delta\Sigma} = \frac{N_c \dot{\theta}_s}{2\pi} \tag{12}$$

The motor's response when utilizing a full-stroke displacement strategy with a first order delta-sigma modulator is shown in Figure 10. The dashed lines indicate the torque reference for the considered displacement.

The figure shows that the resulting winch drum torque shows excessive torque ripples that will cause the load to oscillate. Similar torque ripples are also seen when the other control strategies are considered, thus posing a general problem. However, the ripples can be reduced by utilizing DDMs with a higher number of pistons. Increasing the number of pistons results in a smoother torque output, albeit with a negligible decrease in response time. At the same time, the torque ripples do not affect the analysis of the volumetric efficiency and the findings of the current paper. Therefore, the torque ripples are not considered further in this work but will be addressed in future work.

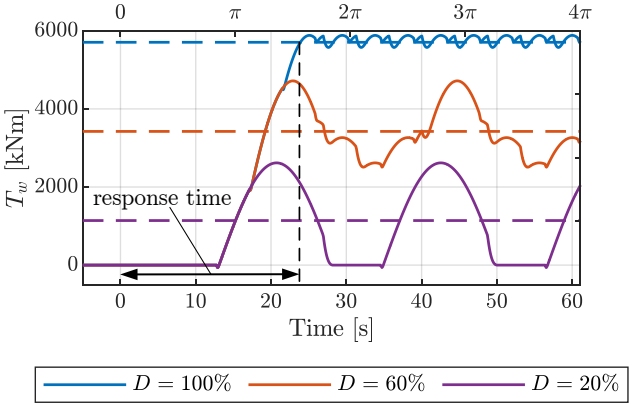


(a)

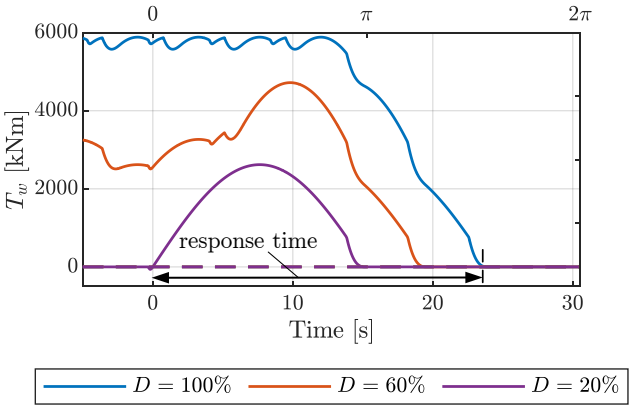


(b)

Figure 10: Torque response for different displacements with full-stroke displacement strategy at 2 rpm. Note the reference signal is given at $t = 0$, as previously mentioned. **(a)** Torque response when the displacement is increased. **(b)** Torque response when the displacement is decreased.

From Figures 10a and 10b, it is seen that the slowest response occurs at the largest displacement change of 100 %, which results in a response time of 23 s which far exceeds the desired value of 1.5 s defined in Section 2. From the top x-axis, it is also observed that the response time corresponds to more than half a revolution. The ideal response time with a full-stroke strategy, from 0 % to 100 % displacement and vice versa, is approximately equal to half a revolution, as the cylinders are activated in sequence (Nordås et al., 2019; Pedersen et al., 2018a). At 2 rpm that corresponds to 15 s; however, there are two delays present that increase the response time. The delays are illustrated in Figure 11, which displays the individual flow through the HPV per cylinder for the 100 % displacement response shown in Figure 10a. Solid lines indicate the actual flow through the HPVs, while the dotted lines indi-

cate the hypothetical flow to the cylinder if the HPV was open. The output of the delta-sigma modulator is denoted as $\alpha_{\Delta\Sigma}$.

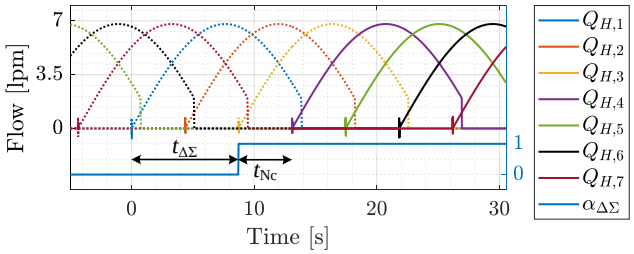


Figure 11: Flow through the HPV for every cylinder of a single digital displacement motor when operating at 2 rpm and for 100 % displacement with a full stroke displacement strategy. Solid lines indicate actual flow while dotted lines illustrate hypothetical flow.

The first delay $t_{\Delta\Sigma}$ is related to the sampling time of the first order delta-sigma modulator introducing a time delay until the digital signal is generated. As shown in Eq. (12), the sampling frequency of the modulator increases proportionally to the shaft speed. Therefore, $t_{\Delta\Sigma}$ decreases as the motor's speed increases. The second delay $t_{N_c}$ is related to the number of pistons and the timing of the displacement reference signal. From Figure 11, it is seen that the modulator sends the signal to activate the 3$^{\text{rd}}$ cylinder at approximately $t = 8.7$ s when the theoretical HPV flow is zero, which corresponds to the opening angle for the HPV. However, as described in Section 4, a full-stroke strategy can only update the state of the pistons at a fixed angle prior to the HPV opening angle. This results in a delay of approximately $t_{N_c} = 4.5$ s, shown in Figure 11, before the 4$^{\text{th}}$ piston can be activated. It is evident that the $t_{N_c}$ delay is reduced for higher angular speeds and a higher number of cylinders. The latter results from the phase shift between the pistons being reduced when more cylinders are distributed around the same shaft. The maximum value of $t_{N_c}$ is given as,

$$t_{N_c,max} = \frac{2\pi}{N_c \dot{\theta}_s} \tag{13}$$

To illustrate the response time of the motors when utilizing a full-stroke displacement strategy at the whole speed range of the drive, Figure 12 is provided. From the figure, It is seen that the torque response time is significantly reduced at higher shaft speeds. A response time below 1.5 s is achieved for shaft speeds higher than 28 rpm.

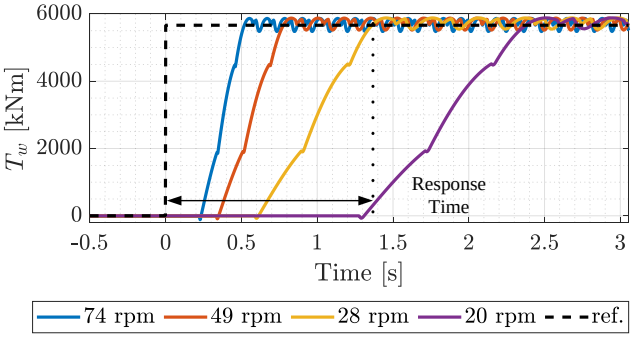


Figure 12: Digital displacement motor response behavior at various shaft speeds with a full-stroke displacement strategy. The reference is stepped from 0 % to 100 %.

## 5.2 Partial-Stroke Response

For partial strokes, the displacement $\mathcal{D}$ is defined as a function of a normalized displacement input $\alpha \in [0, 1]$. The closing angle for the HPV is given by Eq. (14).

$$\theta_{HPV,CL} = \arccos(1 - 2\alpha) \tag{14}$$

$$\mathcal{D} = N_c \frac{V_d}{2\pi} \alpha \tag{15}$$

The torque response with partial strokes is seen in Figure 13. When the displacement is reduced, a partial-stroke strategy updates the HPV closing angle based on Eq. (14), immediately closing any HPV that has exceeded the HPV closing angle. This allows the motors to reduce their torque output near-instantaneously, as shown in Figure 13b. Therefore, the torque response when stepping down the displacement is limited only by the switching time of the valves and is independent of shaft speed. A partial stroke strategy activates each cylinder when its relative shaft angle $\theta_{s,i}$ is zero and varies the HPV closing angle as shown in Eq. (14). Therefore, when the displacement is stepped up from zero to its maximum value, the motor's response is similar to a full-stroke strategy, as shown in Figure 13a. However, it is observed that without the delay imposed by the first order delta-sigma modulator, the motor reaches maximum displacement in half a revolution. At a shaft speed of 2 rpm the winch drive requires 15 s to reach its maximum torque, which is ten times over the desired response time of 1.5 s.

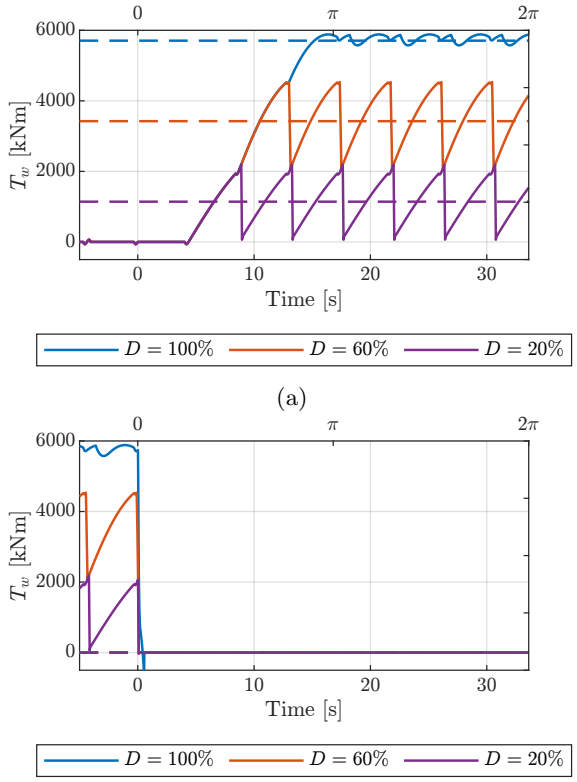


Figure 13: Torque response for different displacements with partial-stroke displacement strategy at 2 rpm. **(a)** Torque response when the displacement is increased. **(b)** Torque response when the displacement is decreased.

The response of the DDM at various shaft speeds when utilizing a partial-stroke strategy is shown in Figure 14.

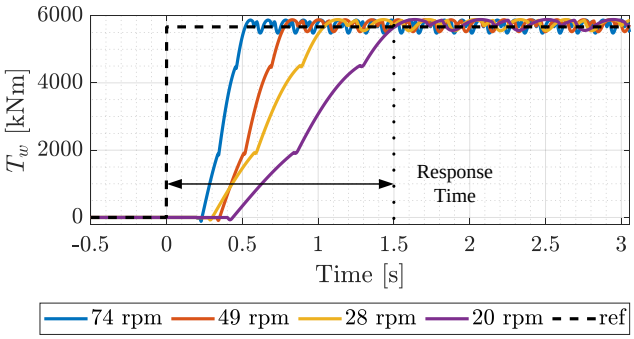


Figure 14: Digital displacement motor response behavior at various shaft speeds with a partial-stroke displacement strategy. The reference is stepped from 0 % to 100 %.

From Figure 14, it is seen that with a partial-stroke strategy, the DDM's response time corresponds to 1.5 s at 20 rpm. As the response time is inversely proportional to the shaft speed with a partial-stroke strategy, it is ensured that the DDM's response is sufficiently fast for shaft speeds above 20 rpm which is verified from Figure 14.

## 5.3 Simplified Sequential Partial-Stroke Response

The s-SPD strategy proposed by Nordås et al. (2019) allows the opening of the HPVs to occur at any angle while the relative shaft angle is above zero, $\theta_{s,i} > 0$, and below the HPV closing angle given by Eq. (14). The torque response of the winch drive when utilizing this method is shown in Figure 15.

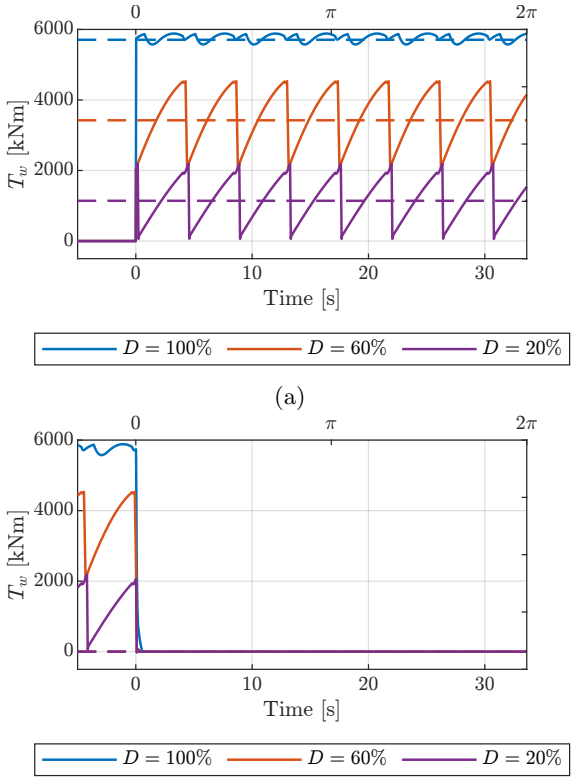


Figure 15: Torque response for different displacements with s-SPD strategy at 2 rpm. **(a)** Torque response when the displacement is increased. **(b)** Torque response when the displacement is decreased.

It is seen that the torque response is near-instantaneous and limited only by the switching time of the valves, regardless of whether the displacement is stepped up or down. With the chosen valves, the response time of the motors when using this method corresponds to approximately 25 ms, which is well below the desired response time of 1.5 s. However, Nordås et al. (2019) did not investigate the energy efficiency

of this method and this is hence left to be investigated. The efficiency of the simplified sequential-stroke displacement strategy is thus investigated in Section 6 along with the efficiency of the other displacement strategies that are considered in this paper.

# 6 Displacement Response Energy Efficiency

This section evaluates the energy efficiency of the considered displacement strategies. Past studies have established the full-stroke strategy as having the highest energy efficiency, while a partial-stroke is characterized by a lower efficiency due to the HPV closing at higher flow rates. The energy efficiency of the s-SPD strategy proposed by Nordås et al. (2019) has not been evaluated yet.

The motor's hydro-mechanical efficiency, such as friction and thermal losses, is disregarded for comparison purposes. Thus, only the volumetric losses introduced by the valves are considered. With this simplification, the energy efficiency per cylinder $\eta_i$ is given by the percentile ratio of the output energy to the input energy. As each motor contains seven cylinders, the resulting energy efficiency for the motor $\eta_m$ is given by summing up both the input and output energy before dividing.

$$\eta_m = \frac{\sum_{i=1}^{N_c} E_{out,i}}{\sum_{i=1}^{N_c} E_{in,i}} 100\ \% \qquad \eta_i = \frac{E_{out,i}}{E_{in,i}} 100\ \% \tag{16}$$

The output and input energy for each cylinder, $E_{out,i}$ and $E_{in,i}$ respectively, are evaluated from the time the displacement signal changes i.e. $t_0 = 0$ s, and until the motor completes a full revolution $T_{\text{rev}} = 2\pi/\dot{\theta}_s$.

$$E_{in,i} = \int_{t_0}^{T_{rev}} Q_{H,i} p_H - Q_{L,i} p_L + \underbrace{\left(\dot{V}_{c,i} + Q_{L,i} - Q_{H,i}\right) p_{c,i}}_{P_{comp,i}} \mathrm{d}t \tag{17}$$

$$E_{out,i} = \int_{t_0}^{T_{rev}} T_{c,i} \dot{\theta}_s \mathrm{d}t \tag{18}$$

The results of the volumetric efficiency evaluation at 2 rpm when the displacement reference is increased are illustrated in Figure 16 for each displacement strategy. When the reference is decreased, all strategies demonstrate nearly 100 % efficiency, with only slight variations beyond the second decimal point, and therefore, the results are not shown. Note that the valves were selected to ensure an energy efficiency of 90 % at the least efficient operation point, which corresponds to a speed of 74 rpm and 25 % displacement, with a partial-stroke displacement strategy. As a result of this choice, both the full-stroke and partial-stroke strategies yield a hydraulic efficiency near 100 %.

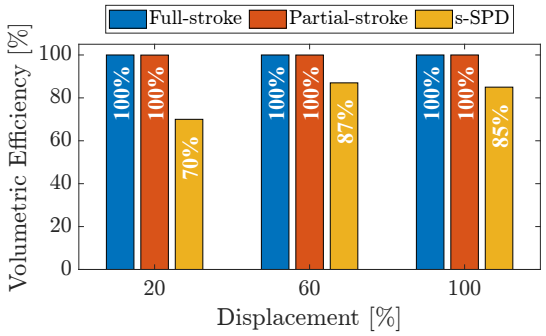


Figure 16: DDM Volumetric efficiency over a cycle when increasing displacement at 2 rpm with different displacement strategies. Notice that the efficiency values are rounded to the nearest integer.

In comparison, the s-SPD strategy switches the valves in the same manner as the partial-stroke strategy when the displacement is reduced. Therefore, the energy efficiency is the same for a descending displacement. However, for an increased displacement, certain HPVs are opened while the corresponding LPVs are closed simultaneously. This essentially short-circuits the high-pressure and the low-pressure lines for the time that the valves require to change states, as shown in Figure 19a. This method results in some cylinders having a drastically reduced efficiency. To illustrate the reduction in energy efficiency, Figure 17 is used.

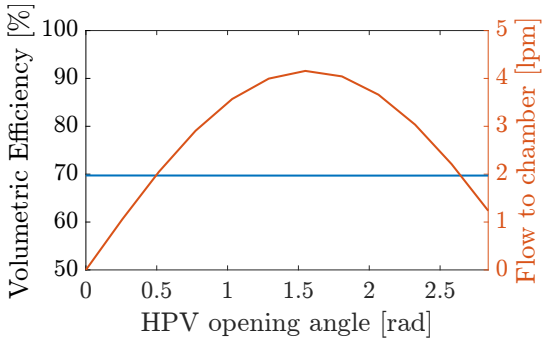


Figure 17: Energy efficiency of a single cylinder using the s-SPD strategy for all HPV closing angles for a shaft speed of 2 rpm.

The figure shows the energy efficiency of a cylinder that changes its displacement from 0 % to 100 % using the s-SPD strategy. The x-axis indicates the angle

where the command to change the displacement was given, thus opening the HPV valve. The orange line indicates the flow to the cylinder prior to opening the HPV. The methodology for obtaining Figure 17 relies on evaluating the energy efficiency of a single cylinder over multiple simulations. Figure 18 shows one iteration of the algorithm for reference. The motor's speed remains constant at 2 rpm, and the HPV closing angle to the maximum, which results from requesting 100 % displacement. The angle where the HPV opens and the LPV closes is indicated by $\theta_{sw}$, and is swiped from zero to the maximum HPV closing angle over multiple iterations. Prior to $\theta_{sw}$, the cylinder is idle, and after the cycle is completed, the cylinder remains active. The energy efficiency is evaluated with Eq. (16) for $i = 1$ and from the time instance where $\theta_s = \theta_{sw}$ and until the shaft completes one revolution. The latter corresponds to the time instance where $\theta_s = \theta_{sw} + 2\pi$.

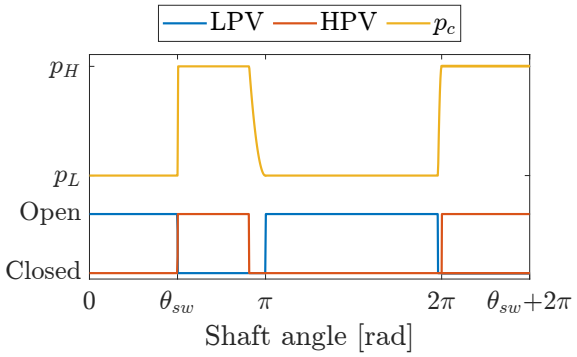


Figure 18: Single iteration of the algorithm used to evaluate energy efficiency for Figure 17.

From Figure 17 it can be concluded that the resulting volumetric efficiency is reduced to 70 %, compared to the near 100 % efficiency offered by either full- or partial-stroke strategies.

## 7 Low-speed Sequential Stroke Strategy

As shown in Section 6, the s-SPD strategy suffers from poor efficiency relative to the full-stroke and partial-stroke strategies. Therefore, in this section, a new sequential partial stroke strategy is proposed to improve energy efficiency while maintaining a fast response. The new strategy is hereby referred to as low-speed sequential partial-stroke displacement strategy (ls-SPD). The proposed method improves the energy efficiency by reducing the time period where the HPV and LPV valves remain open, as shown in Figure 19.

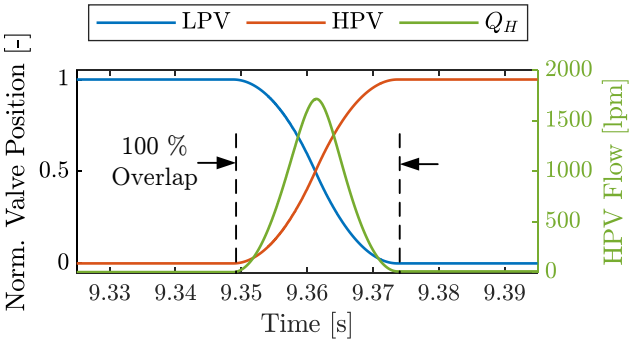


(a)

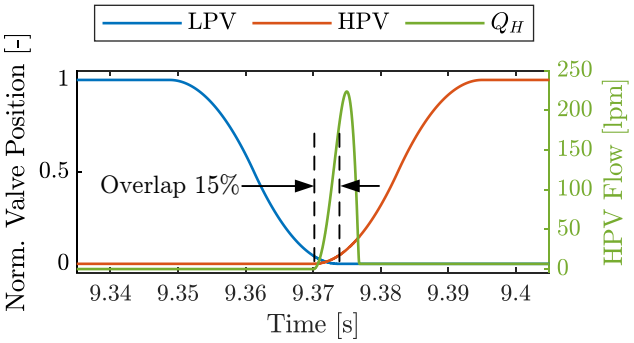


(b)

Figure 19: Illustration of the proposed modification. **(a)** HPV flow when the valves switch states simultaneously, corresponding to 100 % valve overlap. **(b)**Resulting HPV flow when the valve overlap is reduced to 15 %.

The valve overlap is defined as the percentile ratio of the time period where both valves' positions are greater than zero over their switching time. Therefore, an overlap of 100 % corresponds to the valves switching states simultaneously, as shown in Figure 19a. It is seen that with an overlap of 100 % there is a flow of approximately 1800 lpm that flows directly from the high to the low-pressure line, which drastically reduces the efficiency. In Figure 19b the valves overlap is only 15 %. It is noticed that the flow through the HPV has been reduced to 220 lpm. The flow reduction further enables the pressure in high- and low-pressure lines to remain constant. In this study, the supply is assumed to maintain constant pressure in the hydraulic lines regardless of flow demand. In practice, the supply's dynamics are unlikely to be capable of providing such a high flow in the short time that the valves are switching states and will, therefore, also lead to larger fluctuations in pressure. To investigate the resulting energy efficiency from reducing the overlap between the valves throughout the operating speed range of the drive, Figure 20 is provided.

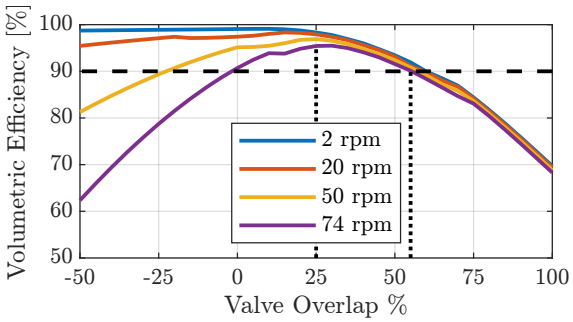


Figure 20: Energy efficiency of a single DDM piston at various speeds using the proposed ls-SPD strategy.

The methodology for producing the figure follows that of Figure 17. However, the shaft angle where the LPV is closed is fixed at $\pi/2$, which corresponds to the highest flow to the chamber and, therefore, the lowest energy efficiency. At every iteration, the overlap of the valves is reduced. An overlap below zero translates to a dead zone from the moment the LPV has closed until the HPV starts to open. For example, at $-50\,\%$, the dead zone equals half the valve switching time $t_s/2$. The process is repeated at various shaft speeds to illustrate the limits of the proposed method. It is seen that when the motor is operating at its minimum speed, the efficiency reaches almost $100\,\%$ when the overlap is below $25\,\%$. However, for higher speeds such as 20 rpm the efficiency starts to decrease when below $15\,\%$ overlap. This is a result of cavitation that occurs due to the chamber pressure dropping rapidly when the position of the LPV becomes too small. This behavior is shown in Figure 21, which illustrates a single iteration of the algorithm used to produce Figure 15.

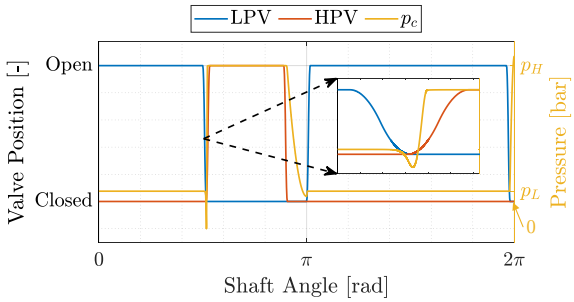


Figure 21: Single iteration of the algorithm used to produce Figure 20, with a shaft speed 20 rpm and a $5\,\%$ overlap.

The iteration under consideration was simulated for a shaft speed of 20 rpm and a valve overlap of $5\,\%$. It is seen that when the LPV's position becomes very small, the chamber pressure drops rapidly, thus leading to cavitation in the cylinder chamber. As the motor's shaft speed increases, cavitation occurs at higher overlap values. This phenomenon results in the ls-SPD strategy being less robust at higher speeds, as the valves must be actuated with increased accuracy to achieve high energy efficiency. This phenomenon is especially clear at the line that corresponds to 74 rpm. From Figure 20, it is observed that in order to maintain efficiency over $90\,\%$ and avoid cavitation, the valve overlap has to remain between $25\,\%$ and $55\,\%$, which is indicated by the vertical dotted lines.

## 8 Results

The DDM's response when utilizing the ls-SPD method is shown in Figure 22 for a shaft speed of 2 rpm and a $15\,\%$ valve overlap.

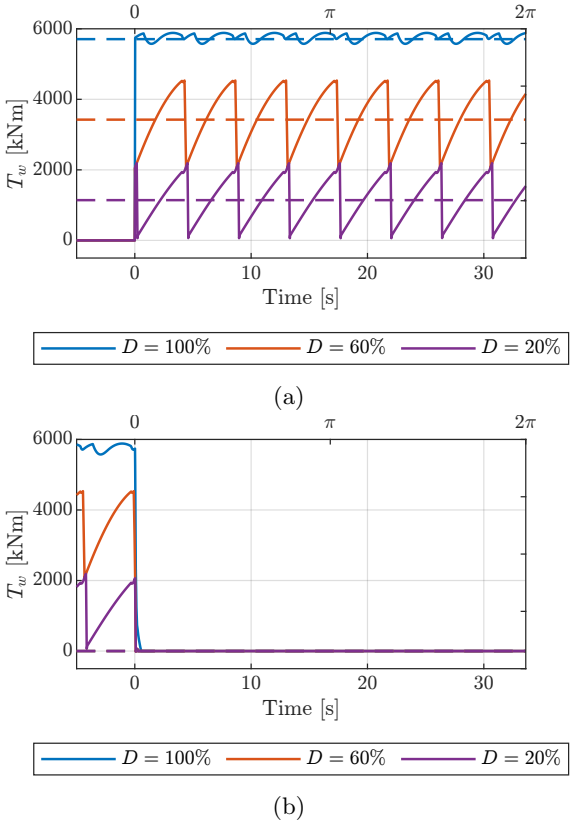


Figure 22: Torque response for different displacements with the ls-SPD strategy at 2 rpm. **(a)** Response when the displacement is increased. **(b)** Response when the displacement is decreased.

By comparing Figure 22 to the response of the s-SPD strategy shown in Figure 15, it is seen that the response time remains nearly identical to that of the s-SPD strategy. At a $15\,\%$ valve overlap, the motor's response time is approximately 50 ms. In comparison with the 25 ms response time offered by the s-SPDS,

both strategies offer a response time well below the desired 1.5 s reference. The volumetric efficiency of the motor's response with the ls-SPD is evaluated following the methodology presented in Section 6 and compared with the efficiency of the s-SPD strategy. The results are shown in Figure 23. The reduction in efficiency at higher speeds and low valve overlap is due to chamber cavitation. It is observed that the proposed method significantly improves energy efficiency compared to the s-SPD strategy when the displacement reference is increased. The most significant improvement occurs at 20 % displacement, where the volumetric efficiency is increased to 100 % compared to the 70 % that corresponds to the s-SPD strategy. At higher displacements, the efficiency is increased from 87 % and 85 % to a 100 %. As mentioned in Section 6, both strategies control the valves in the same manner when the reference is decreased and yield 100 % volumetric efficiency.

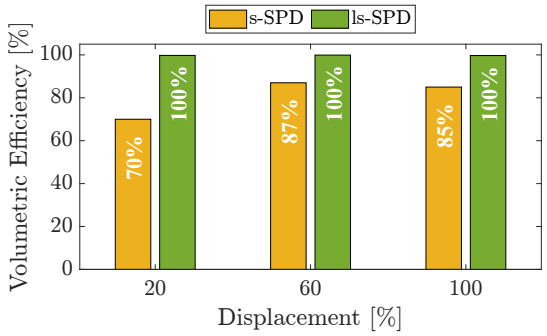


Figure 23: DDM Volumetric efficiency comparison between s-SPD and ls-SPD strategies, over a cycle when changing displacement at 2 rpm when the displacement increases.

## 9 Conclusions

This study analyzed the effectiveness of different displacement control strategies for maintaining the response time of a digital winch drive below 1.5 s and energy efficiency above 90 % without considering hydromechanical losses across its operational range. The proposed drive's parameters and requirements were derived from a commercial offshore hydraulic winch drive system. The requirement of 1.5 s response time was derived from the average response time of the conventional hydraulic motor. This benchmark was employed to evaluate the response time of the various displacement control strategies. The full-stroke displacement strategy demonstrated exceptional volumetric efficiency nearing 100 %, regardless of the given displacement reference. However, the strategy could only meet the desired response time for speeds above 28 rpm. In contrast, the partial-stroke strategy fulfilled the response time criteria for speeds above 20 rpm when the displacement reference was increased. For decreasing displacement reference, the motors could respond instantaneously, independently of the motor's shaft speed. The selected digital valves ensured that the partial-stroke strategy could maintain a minimum efficiency of 90 %. Additionally, the s-SPD strategy proposed by Nordås et al. (2019) enabled the motors to respond instantly regardless of the shaft speed or whether the displacement reference increased or decreased. However, the authors' suggestion of simultaneously switching the valve states substantially reduced energy efficiency and placed strict requirements on the drive's supply. To address this drawback, this paper introduced the ls-SPD strategy, which limits the flow from the high- to the low-pressure line while the valves switch states by delaying the opening of the HPV. The new strategy improved the motor's energy efficiency by up to 43 %. However, at higher shaft speeds, cavitation occurrences reduced the method's robustness, rendering it unsuitable for high-speed operations. Nevertheless, the proposed low-speed sequential-stroke strategy remains advantageous at speeds below 20 rpm, ensuring a fast response and an energy efficiency above 90 %.

## Acknowledgement

This research is funded by The Research Council of Norway, SFI Offshore Mechatronics, project number 237896/O30.

## References

Diinef. Digital Distributor Valve System (DDVS) — Diinef.com. 2023. URL https://www.diinef.com/digital-distributor-valve-system-ddvs.

DNV. DNV-RP-H103: Modelling and Analysis of Marine Operations. 2011.

Farsakoglou, T., Bhola, M., Ebbesen, M. K., Andersen, T. O., and Pedersen, H. C. Valve Specification Requirements For Digital Hydraulic Winch Drives. In *Digital Fluid Power Workshop DFP22*. Edinburgh, Scotland, pages 74–89, 2022.

Heikkilä, M., Tammisto, J., Huova, M., Huhtala, K., and Linjama, M. Experimental Evaluation of a Piston-Type Digital Pump-Motor-Transformer with Two Independent Outlets. In *Fluid Power and Motion Control 2010*. FPMC 2010, Bath, UK, 2010.

Johansen, P., Roemer, D. B., Andersen, T. O., and Pedersen, H. C. Delta-Sigma Modulated Displace-

ment of a Digital Fluid Power Pump. In *Proc. 7th Workshop on Digital Fluid Power*. LCM GmbH, pages 1–9, 2015.

Larsen, H. B., Kjelland, M., Holland, A., and Lindholdt, P. N. Digital Hydraulic Winch Drives. In *BATH/ASME 2018 Symposium on Fluid Power and Motion Control*. American Society of Mechanical Engineers Digital Collection, 2018. doi:10.1115/FPMC2018-8858.

Lindholdt, P. N., Larsen, H. B., and As, D. Digital Distributor Valves In Low Speed Motors - Practical Approach. In *The Ninth Workshop on Digital Fluid Power*. Aalborg, Denmark, page 12, 2017.

Merrill, K. J. *Modeling and Analysis of Active Valve Control of a Digital Pump-Motor*. Ph.D. thesis, Purdue University, United States – Indiana, 2012.

Moslått, G.-A., Padovani, D., and Hansen, M. R. A Control Algorithm for Active/Passive Hydraulic Winches Used in Active Heave Compensation. In *ASME/BATH 2019 Symp. on Fluid Power and Motion Control*. ASME Digital Collection, 2019. doi:10.1115/FPMC2019-1710.

Moslått, G.-A., Padovani, D., and Hansen, M. R. A Digital Twin for Lift Planning With Offshore Heave Compensated Cranes. *Journal of Offshore Mechanics and Arctic Engineering*, 2020. 143(3). doi:10.1115/1.4048881.

Nordås, S. *Using Digital Hydraulics in Secondary Control of Motor Drive*. Ph.D. thesis, Faculty of Engineering and Science, University of Agder, Grimstad, Norway, 2020.

Nordås, S., Beck, M. M., Ebbesen, M. K., and Andersen, T. O. Dynamic Response of a Digital Displacement Motor Operating with Various Displacement Strategies. *Energies*, 2019. 12(9):1737. doi:10.3390/en12091737.

Nørgård, C. *Design, Optimization and Testing of Valves for Digital Displacement Machines*. Ph.D. thesis, Department of Energy Technology, Aalborg University, Aalborg, Denmark, 2017. doi:10.5278/vbn.phd.eng.00013.

NOV. NOV Website. 2022. URL https://www.nov.com/.

Payne, G. S., Kiprakis, A. E., Ehsan, M., Rampen, W. H. S., Chick, J. P., and Wallace, A. R. Efficiency and dynamic performance of Digital Displacement™ hydraulic transmission in tidal current energy converters. *Proceedings of the Institution of Mechanical Engineers, Part A: Journal of Power and Energy*, 2007. 221(2):207–218. doi:10.1243/09576509JPE298.

Pedersen, N. H. *Development of Control Strategies for Digital Displacement Units*. Ph.D. thesis, Department of Energy Technology, Aalborg University, Aalborg, Denmark, 2018.

Pedersen, N. H., Johansen, P., and Andersen, T. Challenges with Respect to Control of Digital Displacement Hydraulic Units. *Modeling, Identification and Control: A Norwegian Research Bulletin*, 2018a. 39:91–105. doi:10.4173/mic.2018.2.4.

Pedersen, N. H., Johansen, P., and Andersen, T. O. LQR Feedback Control Development for Wind Turbines Featuring a Digital Fluid Power Transmission System. In *9th FPNI Ph.D. Symp. on Fluid Power*. ASME Digital Collection, 2016. doi:10.1115/FPNI2016-1537.

Pedersen, N. H., Johansen, P., and Andersen, T. O. Event-Driven Control of a Speed Varying Digital Displacement Machine. In *ASME/BATH 2017 Symp. on Fluid Power and Motion Control*. ASME Digital Collection, 2017. doi:10.1115/FPMC2017-4260.

Pedersen, N. H., Johansen, P., and Andersen, T. O. Optimal control of a wind turbine with digital fluid power transmission. *Nonlinear Dynamics*, 2018b. 91(1):591–607. doi:10.1007/s11071-017-3896-0.

Pedersen, N. H., Johansen, P., and Andersen, T. O. Feedback Control of Pulse-Density-Modulated Digital Displacement Transmission Using a Continuous Approximation. *IEEE/ASME Transactions on Mechatronics*, 2020. 25(5):2472–2482. doi:10.1109/TMECH.2020.2980122.

Roemer, D. B. *Design and Optimization of Fast Switching Valves for Large Scale Digital Hydraulic Motors*. Ph.D. thesis, Department of Energy Technology, Aalborg University, Aalborg, Denmark, 2014.

Rømer, D., Johansen, P., Pedersen, H. C., and Andersen, T. O. Analysis of Valve Requirements for High-Efficiency Digital Displacement Fluid Power Motors. In *Proc. 8th Intl. Conf. Fluid Power Transmission and Control*. World Publishing Cooperation, Hangzhou, China, pages 122–126, 2013.

Williamson, C. and Manring, N. A More Accurate Definition of Mechanical and Volumetric Efficiencies for Digital Displacement® Pumps. In *ASME/BATH 2019 Symposium on Fluid Power and Motion Control*. American Society of Mechanical Engineers Digital Collection, 2019. doi:10.1115/FPMC2019-1668.